Neutron resonance spectroscopy of ^{99}Tc from 3 eV to 150 keV

F. Gunsing, A. Leprêtre, C. Mounier, and C. Raepsaet
CEA/Saclay, F-91191 Gif-sur-Yvette, France

A. Brusegan and E. Macavero
CEC-JRC Institute for Reference Materials and Measurements, B-2440 Geel, Belgium

(Received 24 September 1999; published 7 April 2000)

The total neutron cross section of the nucleus ^{99}Tc from 3 eV to 150 keV has been measured using the time-of-flight technique at the pulsed white neutron source of the Geel Electron Linear Accelerator (GELINA). Up to 10 keV 659 resonances have been resolved and analyzed using the *R*-matrix neutron resonance shape fitting program REFIT. We have attempted to make a division of the resonances into *s* and *p* waves on the basis of their neutron widths. Information on level spacing and neutron strength function has been derived from the resolved resonances. From 10 to 150 keV the average cross section has been analyzed in terms of average level parameters. The results of the present work are compared to previous work, and to the data from the main existing neutron data libraries.

PACS number(s): 25.40.Ny, 25.60.Dz, 25.70.Gh, 25.70.Ef

I. INTRODUCTION

Neutron cross sections in the resonance region have been studied extensively in the past for many nuclei [1,2]. Although experimental work on the interaction of low-energy neutrons with nuclei has for long focused on isotopes of primary interest for nuclear reactor physics, neutron-induced reactions are also important in a number of other fields, including astrophysics and fundamental symmetries.

In recent years an interest has arisen in neutron-nucleus reactions of isotopes related to the transmutation of nuclear waste. The lack of reliable and sufficient data on neutron cross sections of long-living fission products and minor actinides is a major problem in the design of nuclear waste transmutation systems [3].

One of the most important fission products produced in conventional nuclear power plants is the long-living fission product ^{99}Tc, with a half-life of 2.1×10^5 years. After neutron capture, the nucleus ^{100}Tc decays to the stable isotope ^{100}Ru, with a half-life of 16 s. This makes ^{99}Tc a particularly interesting candidate for neutron transmutation [4,5], also given its high geochemical mobility [6].

The possibility of accessing highly excited states in a nucleus with neutrons has largely contributed to the development and verification of the statistical model of the compound nucleus. Information on the level density of highly excited nuclei is obtained directly by an exact counting of excited states above the neutron binding energy, accessible by high-resolution neutron resonance spectroscopy. A systematic examination of neutron resonance data may contribute to a better understanding of fundamental aspects of nuclear structure [7]. The study of resonances in ^{99}Tc allows an investigation of its level density and neutron strength function, which are necessary parameters for neutron cross-section calculations in the unresolved resonance region.

Parity-nonconserving asymmetry effects, associated with a mixing of *s*- and *p*-wave states having the same spin, have been observed up to 10% in *p*-wave resonances of reactions of low-energy polarized neutrons with many nuclei (see Ref. [8], and references therein). The $9/2^+$ nucleus ^{99}Tc may be an interesting candidate for parity violation experiments since the neutron *p*-wave strength function is near a maximum in the mass region of ^{99}Tc. In addition, the relatively high magnetic moment of $5.7\mu_N$ for ^{99}Tc is very advantageous for polarizing a sample of it, allowing the possible observation of time-reversal invariance nonconservation. For the analysis and interpretation of these kind of measurements, high-quality neutron resonance spectroscopic information is necessary [9].

Nucleosynthesis in stellar environments is used in stellar model calculations to explain the abundances of the elements [10,11]. The observed abundance of ^{99}Tc is a measure of the evolution of asymptotic giant branch stars [12,13]. The Maxwellian averaged neutron capture cross section of ^{99}Tc is a crucial input parameter to determine the ^{99}Tc abundance in *s*-process nucleosynthesis calculations.

Although relatively few measurements of the nucleus ^{99}Tc are reported in the literature as compared to other isotopes, several measurements of the resonance parameters of ^{99}Tc have been performed in the past. After some early work [14,15], resonance parameters in the region from thermal up to 1 keV were given by Watanabe and Reeder [16] and Adamchuck *et al.* [17]. A measurement by Chou and Werle [18] using a lead slowing down spectrometer, gave average properties up to 50 keV, and parameters for the first two large resonances. Little and Block [19] gave average values up to 80 keV. Fischer *et al.* [20] studied the two first large resonances at 5.6 and 20.3 eV. Finally Macklin [21] made an extensive study of the capture cross section from 2.65 up to 2000 keV. A recent evaluation [22] of the existing data showed several inconsistencies, and an interest in more precise resonance parameters exists [23]. For these reasons we have decided to study the neutron-nucleus interaction of ^{99}Tc more in detail by means of the investigation of the total cross section in the energy range from 3 eV up to 150 keV.

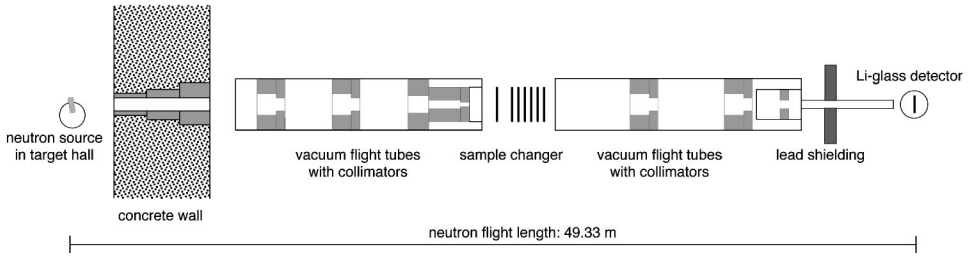

FIG. 1. A schematic view of the transmission setup used. The flight tubes have a diameter of 50 cm, while the flight length is about 50 m.

II. EXPERIMENTAL METHOD

A. Neutron source

The total cross-section measurements of ^{99}Tc were performed using the time-of-flight technique at the pulsed neutron facility GELINA (Geel Electron Linear Accelerator) of the Institute for Reference Materials and Measurements (IRMM). A detailed description of the accelerator and its neutron producing target can be found elsewhere [24,25]. Two energy ranges have been investigated. One experiment was set up to cover the energy range from 3 to 600 eV using two thin samples, with the Geel linac operating to provide electron bursts of 100 MeV average energy and 15 ns width at a repetition frequency of 200 Hz and an average beam current of 20 μA. For the experiment with a thick sample, intended for a measurement from 20 eV to 150 keV, the linac was functioning at 800 Hz with an average beam current of 60 μA and a pulse width of 2 ns, obtained with a pulse compressing magnet system [26]. Neutrons were produced by (γ,n) and (γ,f) reactions, induced via bremsstrahlung from the electron beam hitting a rotating uranium target. The fast neutron spectrum from the target was moderated to a white spectrum by water contained in a beryllium canning of 4 cm thick, situated beneath and above the target. The partially thermalized neutrons scattered from the moderators were collimated into the flight path through evacuated aluminum pipes of 50 cm diameter with collimators consisting of borated wax, copper, and lead, placed at regular distances. A shadow bar made of copper and lead was placed in front of the uranium target, preventing fast neutrons from the rotary target from going into the flight path and diminishing the gamma flash. In order to absorb slow neutrons that otherwise overlap with the next machine cycle, a cutoff filter of $^{10}B_4C$ was placed in the neutron beam. For the low-energy experiments we used 0.110 g/cm^2 of ^{10}B, while for the high-energy experiments we used a 0.490 g/cm^2 ^{10}B filter.

B. Samples

Three ^{99}Tc samples, disc shaped with a diameter of 50 mm, with total amounts of 3.1337, 5.3963, and 80.1853 g ^{99}Tc (nominal thicknesses of 0.16, 0.28, and 4.0 g/cm^2, respectively), as well as dummy samples, have been prepared for the transmission experiments at the sample preparation group of the IRMM. The two thin samples were composed of a mixture of Tc_4Al_{11} obtained from the Institute for Transuranium Elements (ITU) Karlsruhe and 80% natural sulfur powder, pressed into pallets for a homogeneous distribution of the technetium. The thick sample consisted of pure metal technetium also obtained from ITU Karlsruhe. Analysis of the chemical composition of the technetium material showed several trace elements. The most important ones are Fe (30 ppm), Re (25 ppm), and W (6 ppm). Other elements were present in quantities less than 5 ppm. The amount of isotopes with masses between 237 and 241 was less than 1 ppm. All samples were contained in aluminum cans with a diameter of 50 mm, and sealed with epoxy resin. In the experiments, samples of 0.16 and 0.28 g/cm^2 were used together as a sample of 0.44 g/cm^2 thickness.

C. Setup of the transmission experiment

The experimental equipment of the transmission setup has been used frequently for high-resolution transmission measurements [27,28]. Here we briefly describe the main points. At a distance of 23 m from the neutron source the ^{99}Tc sample was placed in an automatic sample changer, driven by the data acquisition system. Data were taken in many cycles lasting about 1 h each. Each cycle consisted of four measurement sequences during which data were recorded. During two sequences the neutron flux was measured with the Tc sample in and out of the beam. During two additional sequences, several filters were put in the beam, with and without the Tc samples, for the determination of the background using the ''black resonance'' method. Black resonances are strong resonances from isotopes put in the beam, removing all neutrons around the resonance energy. We used filters of W, Mo, Co, Bi, and Mn for experiments at low energy, and samples of Bi, Co, Mn, Na, S, and Si for measurements at high energy. In addition, 8 mm of Pb was put permanently in the beam to decrease the γ flash.

The neutron beam passing through the sample and filters was further collimated and detected by a NE912 lithium glass of 1/4 in. thick, and with a diameter of 6 in., placed at a distance of 49.33 m from the neutron source. In this way the solid angle subtended by the detector becomes negligible, and only neutrons which have not undergone an interaction with the sample are detected. The lithium glass was placed in an aluminum sphere with an inside coating of a seven layer $BaSO_4$ light reflector. The sphere was connected through a boron-free quartz window to a 5 in. EMI9823KQB photomultiplier, installed orthogonally and out of the neutron beam. The schematic view of the experimental setup is shown in Fig. 1.

The anode signals of the photomultiplier were electronically processed and, if the pulse height was in coincidence with a preset window corresponding to the scintillation of the glass due to the ^{6}Li(n,α) reaction, sent to a 23-bit, multiple stop fast-time digitizer, developed at the IRMM. These events, converted to a neutron time of flight, were binned on-line into a 32 k time-of-flight spectrum with channel widths varying from 2 to 2048 ns and stored by the data-acquisition system for further analysis. The detector and electronics were situated in a climatized flight path station with constant temperature. From the position of the peak of the amplitude pulse spectra, which were recorded for each cycle together with the time-of-flight spectra, we found a variation of the gain of 1.7% standard deviation. Data were recorded during 70, 150, and 450 h of effective beam time in 34, 69, and 572 cycles for three ^{99}Tc samples of 0.16, 0.44, and 4.0 g/cm^2 thicknesses, respectively.

D. Data reduction and transmission

The transmission of an incident beam of neutrons on a sample with a thickness of n atoms per barn is directly related to the total neutron cross section $\sigma_T(E)$ by the relation

$$T(E)=e^{-n\sigma_T(E)}=\frac{\varphi_1(E)}{\varphi_2(E)}=N\frac{S_{\rm in}(E)-B_{\rm in}(E)}{S_{\rm out}(E)-B_{\rm out}(E)}, \qquad (1)$$

where the ratio of the attenuated and incident neutron fluxes $\varphi_1(E)$ and $\varphi_2(E)$ is defined as the transmission factor $T(E)$. Since it is quite difficult to measure both fluxes simultaneously, in a standard transmission experiment the fluxes are measured alternatingly with a sample in and out of the neutron beam. The transmission factor is then calculated as the ratio of the two time-integrated spectra $S(E)$, corrected for the estimated background $B(E)$, and normalized to the ratio N of the integrated intensities of the incident neutron beam during the in and out cycles.

Since the neutron flux, like any particle beam, varies in the course of the measurement time in intensity and energy profile, the alternating sequence of measurements was repeated many times in order to approach an identical incoming average neutron flux for the two sequences. For the normalization we had the information of several neutron flux monitors available, measuring the energy- and time-integrated neutron flux for each cycle as well as the duration of each cycle in terms of the number of accelerator cycles. Four BF_3 detectors were located at different positions in the target hall and in the case of the low-energy measurements; in addition, a lithium-glass monitor was placed in the neutron beam at about 30 cm in front of the sample. The normalization was taken as the ratio of the flux monitor counts during the time that the sample was in (or out) of the neutron beam. The raw time-of-flight counting spectra were corrected for dead time, which was electronically fixed at 3 μs for the low-energy measurements and was on the average 1.9 μs for the high-energy measurements.

We parametrized the background as a smooth function of the time of flight in the form of a constant added to two exponentials for the low-energy measurements, and three exponentials for the high-energy measurements. This function was fitted to the points corresponding to the black resonances, and then scaled to the spectra $S_{\rm in}$ and $S_{\rm out}$ by means of permanent black resonances. This was bismuth at 800 eV in the low-energy measurement and sulfur at 112 keV in the high-energy measurement. This background was then subtracted from the spectra corresponding to the sample in and out of the beam, respectively. The transmission factor was derived as the ratio of these spectra, normalized by the ratio of the monitor counts of the ''in'' and ''out'' sequences.

The in-house developed data processing package AGS (Analysis of Geel Spectra) [29,30] was used to apply the various spectrum manipulations as dead time correction, normalization, and background fitting and subtraction on the recorded histograms. Using this package, the initial raw counting spectra are considered to have only statistical counting errors and no correlated uncertainties. The mathematical operations on the spectra may introduce correlations which are taken into account and propagated to the next step. Because of the known mathematical uncertainty propagation, it is possible to store the covariance matrix in the form of vectors, one for each correlated component. Then the matrix formed by the sum of the products of each vector and its transpose is the covariance matrix. In this way the transmission factor is derived with its covariance matrix resulting from these operations with a considerable gain in covariance storing and handling.

III. ANALYSIS OF THE RESOLVED RESONANCES

A. Resonance parameters

The large fluctuations of the neutron cross sections in the resonance region, due to the excitation of nuclear levels in the compound nucleus, makes a parametrization indispensable for practical usage of neutron cross sections. The measured data are not a total cross section, but an energy-dependent transmission factor, affected by experimental resolution and Doppler broadening. The advantage of parametrized compound levels is that a desired neutron cross section, partial or total at a given temperature, can be reconstituted from a limited set of parameters.

The interaction of the neutron with the nucleus can be suitably described with R-matrix theory [31–34]. For neutron-induced reactions this formalism divides the configuration space in an external region with the neutron and the nucleus as two free particles with known wave functions, and an internal region where the compound nucleus with unknown wave function exists. The unknown wave function of the compound nucleus is described as an expansion of its eigenstates, parametrized by their energies and decay amplitudes. Neutron cross sections, which can easily be expressed in terms of the collision matrix, can in this way be related to the resonance parameters of the R matrix.

The total cross section for the entrance channel c, referred to by a given constellation of the relative orbital momentum and the spins of the incoming neutron and the target nucleus, is related to the collision matrix U_{cc} by

$$\sigma_c = 2\pi\lambda\!\!\!^{-2} g_c (1 - \mathrm{Re}\, U_{cc}). \quad (2)$$

In the limiting case of a single, isolated $l=0$ resonance at low $(R/\lambda\!\!\!^{-} \ll 1)$ energy E_0 and with capture and elastic scattering as the only open channels, the total cross section can be expressed in the single-level Breit-Wigner form as [32,35,36]

$$\sigma_T(E) = 4\pi R'^2 + \pi\lambda\!\!\!^{-2} g \left(\frac{4\Gamma_n (E-E_0) R'/\lambda\!\!\!^{-} + \Gamma_n^2 + \Gamma_n \Gamma_\gamma}{(E-E_0)^2 + (\Gamma_n + \Gamma_\gamma)^2/4} \right), \quad (3)$$

where Γ_n is the neutron width, Γ_γ is the radiative width, g is the statistical spin factor defined in Eq. (7), and $\lambda\!\!\!^{-}$ is the reduced de Broglie wavelength of the neutron.

The first term is the effective potential scattering cross section $\sigma_p = \Sigma_l 4\pi g_l \lambda\!\!\!^{-2} \sin^2\phi_l$. For neutron energies below 10 keV in ^{99}Tc, the partial wave contributions from $l \geqslant 1$ are negligible. The hard-sphere phases ϕ_l depend on the channel radius which divides the internal and external regions in the *R*-matrix formalism. For the channel radius, which is not necessarily equal for different channels, a distance should be taken where the nuclear interaction between the neutron and the target nucleus can be neglected, and so is at least slightly larger than the nuclear radius. In practice an effective potential scattering radius R' is determined at low energies where only *s* waves contribute to the potential scattering cross section by $\sigma_p = 4\pi R'^2$. This effective radius includes a convenient channel radius as well as the possible effects of distant levels. At higher energies it is customary to have different radii R'_l for each partial wave.

The first term within the brackets in Eq. (3) corresponds to the interference of potential and resonance scattering, resulting in a dip in the total cross section at the low-energy side of the resonance. The other two terms correspond to resonance scattering and capture, respectively. In the nonfissile nucleus ^{99}Tc the total neutron cross section at low energies is the sum of the scattering cross section and the capture cross section. The first inelastic scattering channel opens for the $7/2^+$ level at 140 keV.

We have used the *R*-matrix neutron resonance-shape-fitting program REFIT [37] to fit resonance parameters up to 10 keV. Three data sets were available: two sets from 3 to 600 eV with thicknesses of 0.16 and 0.44 g/cm^2, and one set from 15 eV to 150 keV with a sample thickness of 4.0 g/cm^2.

TABLE I. The large $l=0$ resonances for which both Γ_γ and $g\Gamma_n$ could be determined together with their correlation coefficients. The errors are the statistical uncertainties resulting from the fit.

E_0 (eV)	J	Γ_γ (meV)	$g\Gamma_n$ (meV)	$\rho(\Gamma_\gamma,\Gamma_n)$
5.6	5	146.4±0.9	1.89±0.01	−0.86
20.3	4	154.8±0.8	3.75±0.01	−0.49
39.8	5	121.4±2.1	0.59±0.01	−0.17
56.7	4	139.9±1.8	1.75±0.01	−0.54
111.2	5	132.9±1.9	5.46±0.03	−0.52
123.8	4	143.4±3.3	1.84±0.01	−0.44
163.0	5	144.4±1.6	31.65±0.16	−0.77
182.1	4	160.0±2.1	30.19±0.17	−0.79
191.7	5	147.2±2.2	20.00±0.13	−0.67

The resolution of the neutron time-of-flight spectrometer is modeled by a convolution of its components. It takes into account the initial electron pulse shape and target decay, the material and geometry of the water moderator, the channel width of the time bins, and the resolution of the detector used. We used a parametrization of the resolution function optimized for the flight path used [27,28,38]. For broadening due to the Doppler effect, we used a free-gas model with an effective temperature [39].

The data up to 600 eV could be analyzed with a simultaneous fit, and we checked the consistency of the data sets with separated fits. From the fits we obtained an effective temperature of about 313 K, slightly above room temperature, which we kept constant throughout the analysis.

The potential scattering radius can be determined for certain nuclei using the interference between the potential and resonance scattering. In the case of ^{99}Tc, the interference is too weak for the sample thicknesses used to allow a determination of the potential scattering radius.

However, due to the relatively large level spacing in the compound nucleus ^{100}Tc and the subsequent large off-

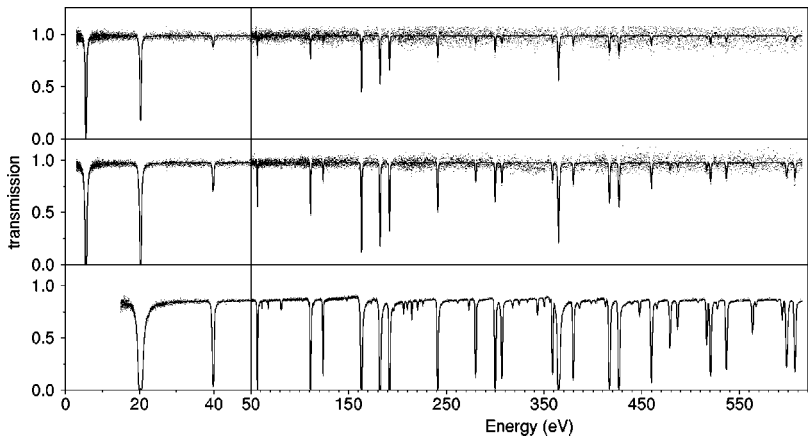

FIG. 2. The result of a simultaneous fit of the data from three samples with thicknesses of 0.16, 0.44, and 4.0 g/cm^2 in an energy range from 3 to 600 eV. The energy scale is enlarged at the left side of the vertical line.

resonance zones at low neutron energies, we could determine R' from a fit of the energy range up to 200 eV. We obtained a value of 7.17 ± 0.13 fm for the effective potential scattering radius, which also was kept constant further in the analysis. This value of R' is in between the value of 6.0 fm in the evaluated nuclear data library of the OECD Nuclear Energy Agency JEF-2.2 [40] and the Japanese evaluated nuclear data library JENDL-3.2 [41] and the value of 7.9 fm in the United States evaluated nuclear data file ENDF/B-VI [42].

The uncertainty on R' includes a statistical error of 0.8% from the fit. Systematic errors are mainly due to normalization and background effects. An error of 0.6% has been attributed to the background. The distribution of the normalization factor for the ensemble of the 572 cycles has a standard deviation of 1.2%, resulting in a 0.06% error on the average value, taking into account autocorrelation and jackknife bias removal [43,44]. Nevertheless, we adopt a relative uncertainty of 0.5% in the normalization which propagates as a 1.5% error on the potential scattering radius.

The radiation width Γ_γ should be relatively constant from one resonance to another for a medium mass nucleus as ^{99}Tc, as a consequence of the many levels available to the resonance state for γ decay. However, the average radiation width of p waves may be different from that of s-wave resonances. At low energies the neutron width Γ_n is much smaller than Γ_γ. In addition the broadening due to the Doppler effect and the machine resolution, which is about 750-meV full width at half maximum at a neutron energy of 200 eV, is still small enough to determine Γ_γ by shape fitting below that energy. We determined the radiative width for nine large, isolated resonances up to 200 eV. The weighted average is 146.9 meV, with a weighted standard deviation of the distribution of 7% of the average value. Numerical values are given in Table I. This average value of Γ_γ was then kept fixed for all other resonances, including the p-wave resonances, to determine the neutron widths Γ_n.

For the nucleus ^{99}Tc the spin of the resonance states cannot be determined from the shape of the resonances due to the high spin of 9/2, resulting in nearby values of g. Moreover, the interference between the potential and resonance scattering is also too small to derive spin information. Spin information is important to account for level-level interference of nearby resonances of the same spin and parity. In other cases, as for example parity violation in neutron resonances, the spin of the resonance is also an important parameter [9]. But often resonance spins are unknown, and are fixed at a given value while fitting the other resonance parameters. A separate study of the resonance spins of ^{99}Tc for this purpose was started [45], using the method of low-level population [46,47]. The resonance spins for 51 s-wave resonances up to 1.5 keV were determined and given in the table. To the other resonances, all with $l \leqslant 1$, the spins were assigned randomly, $J=4$ or 5 for s waves and $J=3,\ 4,\ 5$ or 6 for p waves, according to a level density with a $2J+1$ spin dependence as a rough approximation of the spin distribution [48].

The thermal cross section, which is the cross section for neutrons with a speed of 2200 m/s, corresponding to a kinetic energy of 25.3 meV, is the resulting cross section of the tails of all resonances, including ''negative'' resonances corresponding to levels below the neutron binding energy. For the fitting of the distant level parameter R^∞, related to the potential scattering radius, it is necessary to have several negative resonances, even if for the description of the cross section down to thermal energies only one negative resonance would be sufficient. We introduced 20 s-wave resonances with negative energy, spaced by 15 eV, with a fixed radiation width of 150 meV and a fixed neutron width according to a neutron strength function $S_0 = 0.5 \times 10^{-4}$. From the negative resonances we fitted the neutron width of the one closest to zero, at -15 eV, to match the thermal neutron capture cross section of 22.9 ± 1.3 b from Ref. [49]. Once we obtained the value of R^∞ from the fit with many negative resonances, we fixed R^∞, removed all negative resonances but one, and adjusted its neutron width for a good description of the thermal point.

In Fig. 2 the result of simultaneous fits in the energy range from 3 to 600 eV of the data for the three sample thicknesses is shown. For the energy range from 0.6 to 150 keV, data have been taken only for the thickest sample. The result of the fits is shown in Fig. 3. Part of the resonance parameters are given in Table II.

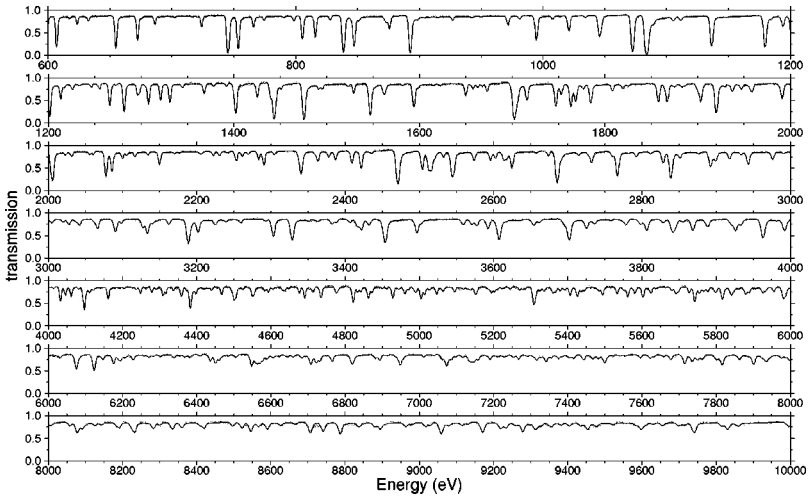

FIG. 3. The result of the fit of the data from the sample with a thickness of 4.0 g/cm^2 in an energy range from 0.6 to 10 keV.

TABLE II. The resonances for which the parameters have been determined. The error on the resonance energy E_0 includes a 1 cm error on the flight length. The fixed radiation width was taken as $\Gamma_\gamma = 146.9$ meV, except for the resonances from Table I. The spin values for 51 resonances up to 1.5 keV are taken from Ref. [45], while the other spins, given between brackets, have been assigned randomly according to a $2J+1$ level density. The parity assignment is based on the neutron widths, and is given with the probability for the resonance being a p wave. From the measured quantity $g\Gamma_n$ we give the neutron width Γ_n together with the statistical uncertainties resulting from the fit. The systematic errors, discussed in the text, are estimated at 3.5%. Note that only parameters up to 1 keV are given in the table. The complete table with all 659 resonances can be requested from the OECD/NEA databank.

E_0 (eV)	J	l	P $(l=1\|g\Gamma_n)$	Γ_γ (meV)	Γ_n (meV)	E_0 (eV)	J	l	P $(l=1\|g\Gamma_n)$	Γ_γ (meV)	Γ_n (meV)
-15.00 ± 0.01	[5]	0		150.0	14.09 ± 0.15	361.45 ± 0.03	[5]	0	0.60	146.9	1.03 ± 0.04
5.58 ± 0.01	5	0	0.00	146.5	3.45 ± 0.01	362.69 ± 0.02	[4]	0	0.20	146.9	1.97 ± 0.04
14.60 ± 0.02	[3]	1	0.81	146.9	0.02 ± 0.01	364.93 ± 0.01	5	0	0.00	146.9	142.40 ± 0.39
20.27 ± 0.01	4	0	0.00	155.0	8.37 ± 0.02	379.84 ± 0.01	5	0	0.00	146.9	20.94 ± 0.07
22.39 ± 0.03	[5]	1	0.95	146.9	0.01 ± 0.01	386.12 ± 0.04	[5]	1	0.85	146.9	0.63 ± 0.03
39.84 ± 0.01	5	0	0.00	122.7	1.08 ± 0.01	398.30 ± 0.07	[3]	1	0.92	146.9	0.58 ± 0.05
56.68 ± 0.01	4	0	0.00	141.1	3.90 ± 0.02	403.00 ± 0.08	[3]	1	0.93	146.9	0.49 ± 0.05
58.71 ± 0.04	[6]	1	0.97	146.9	0.02 ± 0.01	410.42 ± 0.43	[4]	1	0.94	146.9	0.08 ± 0.04
61.43 ± 0.01	[3]	1	0.85	146.9	0.10 ± 0.01	412.93 ± 0.03	[5]	1	0.77	146.9	0.91 ± 0.03
66.06 ± 0.06	[5]	1	0.97	146.9	0.02 ± 0.01	416.82 ± 0.01	4	0	0.00	146.9	64.38 ± 0.24
67.66 ± 0.01	[4]	1	0.80	146.9	0.10 ± 0.01	426.54 ± 0.01	5	0	0.00	146.9	60.85 ± 0.23
80.96 ± 0.01	[3]	1	0.77	146.9	0.17 ± 0.01	433.21 ± 0.18	[6]	1	0.94	146.9	0.15 ± 0.03
81.73 ± 0.01	[6]	1	0.80	146.9	0.09 ± 0.01	439.77 ± 0.11	[3]	1	0.93	146.9	0.46 ± 0.06
102.84 ± 0.05	[4]	1	0.96	146.9	0.05 ± 0.01	447.70 ± 0.02	[5]	0	0.18	146.9	2.22 ± 0.04
109.19 ± 0.03	[3]	1	0.94	146.9	0.11 ± 0.01	459.92 ± 0.01	4	0	0.00	146.9	41.82 ± 0.15
111.22 ± 0.01	5	0	0.00	134.3	9.94 ± 0.03	465.51 ± 0.04	[6]	1	0.78	146.9	0.87 ± 0.04
114.21 ± 0.03	[5]	1	0.95	146.9	0.07 ± 0.01	478.77 ± 0.01	4	0	0.00	146.9	12.72 ± 0.08
123.77 ± 0.01	4	0	0.00	145.1	4.11 ± 0.01	480.40 ± 0.10	[4]	1	0.91	146.9	0.60 ± 0.06
148.34 ± 0.04	[3]	1	0.95	146.9	0.12 ± 0.01	486.58 ± 0.01	5	0	0.00	146.9	5.35 ± 0.05
161.27 ± 0.02	[5]	1	0.88	146.9	0.18 ± 0.01	497.44 ± 0.48	[6]	1	0.94	146.9	0.07 ± 0.04
163.01 ± 0.01	5	0	0.00	144.3	57.82 ± 0.14	507.69 ± 0.10	[6]	1	0.92	146.9	0.36 ± 0.04
173.15 ± 0.04	[4]	1	0.94	146.9	0.15 ± 0.01	516.45 ± 0.01	4	0	0.00	146.9	13.15 ± 0.08
177.49 ± 0.07	[6]	1	0.96	146.9	0.06 ± 0.01	520.56 ± 0.01	5	0	0.00	146.9	29.53 ± 0.11
182.09 ± 0.01	4	0	0.00	160.4	67.33 ± 0.16	527.39 ± 0.04	[4]	1	0.72	146.9	1.70 ± 0.07
191.71 ± 0.01	5	0	0.00	148.8	36.40 ± 0.11	536.61 ± 0.01	4	0	0.00	146.9	30.45 ± 0.12
196.36 ± 0.03	[3]	1	0.89	146.9	0.35 ± 0.02	563.23 ± 0.01	5	0	0.00	146.9	7.97 ± 0.07
206.41 ± 0.01	[4]	0	0.45	146.9	0.69 ± 0.01	567.09 ± 0.05	[6]	1	0.81	146.9	1.03 ± 0.05
209.96 ± 0.02	[4]	1	0.74	146.9	0.49 ± 0.01	588.80 ± 0.12	[6]	1	0.91	146.9	0.44 ± 0.05
214.83 ± 0.01	[4]	0	0.05	146.9	1.19 ± 0.02	593.75 ± 0.01	4	0	0.01	146.9	6.20 ± 0.08
220.62 ± 0.01	[5]	0	0.66	146.9	0.49 ± 0.01	598.17 ± 0.01	5	0	0.00	146.9	26.11 ± 0.18
226.00 ± 0.03	[4]	1	0.91	146.9	0.29 ± 0.02	599.54 ± 0.04	[5]	0	0.20	146.9	3.26 ± 0.14
241.21 ± 0.01	4	0	0.00	146.9	37.94 ± 0.13	606.76 ± 0.01	4	0	0.00	146.9	37.60 ± 0.15
261.66 ± 0.05	[3]	1	0.93	146.9	0.33 ± 0.03	617.32 ± 0.07	[3]	1	0.87	146.9	1.47 ± 0.10
273.17 ± 0.02	[4]	0	0.66	146.9	0.79 ± 0.03	623.49 ± 0.02	[4]	0	0.05	146.9	5.49 ± 0.09
279.98 ± 0.01	4	0	0.00	146.9	15.02 ± 0.05	630.53 ± 0.17	[5]	1	0.92	146.9	0.47 ± 0.08
282.32 ± 0.14	[6]	1	0.95	146.9	0.08 ± 0.02	632.56 ± 0.03	[5]	0	0.53	146.9	2.39 ± 0.08
299.98 ± 0.01	4	0	0.00	146.9	36.94 ± 0.13	654.71 ± 0.01	4	0	0.00	146.9	46.47 ± 0.18
305.10 ± 0.03	[5]	1	0.79	146.9	0.59 ± 0.02	672.24 ± 0.01	5	0	0.00	146.9	21.50 ± 0.11
306.81 ± 0.01	5	0	0.00	146.9	14.32 ± 0.05	675.41 ± 0.08	[4]	1	0.87	146.9	1.33 ± 0.10
317.72 ± 0.03	[6]	1	0.78	146.9	0.53 ± 0.02	686.23 ± 0.02	[5]	0	0.05	146.9	5.21 ± 0.09
324.64 ± 0.04	[5]	1	0.87	146.9	0.46 ± 0.02	689.99 ± 0.24	[3]	1	0.92	146.9	0.58 ± 0.13
333.19 ± 0.06	[6]	1	0.92	146.9	0.24 ± 0.02	699.33 ± 0.62	[6]	1	0.93	146.9	0.14 ± 0.07
343.21 ± 0.01	[5]	0	0.13	146.9	1.62 ± 0.03	702.16 ± 0.12	[5]	1	0.90	146.9	0.77 ± 0.09
350.15 ± 0.02	[3]	1	0.69	146.9	1.35 ± 0.04	716.61 ± 0.20	[6]	1	0.92	146.9	0.43 ± 0.08
356.11 ± 0.03	[5]	1	0.84	146.9	0.61 ± 0.03	720.69 ± 0.12	[6]	1	0.90	146.9	0.67 ± 0.08
358.65 ± 0.01	4	0	0.00	146.9	19.61 ± 0.06	724.09 ± 0.01	[5]	0	0.00	146.9	8.27 ± 0.10

TABLE II. *(Continued).*

E_0 (eV)	J	l	P $(l=1\|g\Gamma_n)$	Γ_γ (meV)	Γ_n (meV)	E_0 (eV)	J	l	P $(l=1\|g\Gamma_n)$	Γ_γ (meV)	Γ_n (meV)
727.19±0.38	[4]	1	0.93	146.9	0.34±0.11	872.13±0.13	[3]	1	0.71	146.9	4.28±0.52
745.37±0.01	4	0	0.00	146.9	114.70±0.48	873.59±0.08	[4]	0	0.31	146.9	5.90±0.37
753.60±0.01	4	0	0.00	146.9	62.96±0.26	875.92±0.02	[5]	0	0.00	146.9	12.93±0.17
766.09±0.01	[4]	0	0.00	146.9	10.87±0.14	892.72±0.01	4	0	0.00	146.9	139.30±0.60
774.51±0.04	[5]	0	0.59	146.9	2.89±0.10	898.52±0.10	[5]	1	0.85	146.9	1.64±0.14
790.62±0.12	[4]	1	0.89	146.9	1.21±0.13	904.15±0.29	[5]	1	0.91	146.9	0.60±0.14
798.64±0.03	[4]	0	0.38	146.9	4.82±0.14	915.31±0.22	[3]	1	0.91	146.9	1.25±0.22
805.59±0.01	5	0	0.00	146.9	27.43±0.15	927.00±0.05	[4]	0	0.56	146.9	4.72±0.18
815.91±0.01	5	0	0.00	146.9	24.64±0.15	942.91±0.14	[5]	1	0.88	146.9	1.30±0.15
828.04±0.04	[4]	0	0.58	146.9	3.96±0.14	950.09±0.39	[5]	1	0.92	146.9	0.48±0.15
838.71±0.01	4	0	0.00	146.9	119.10±0.50	971.80±0.02	[5]	0	0.01	146.9	10.75±0.17
844.94±0.08	[5]	1	0.79	146.9	2.09±0.13	981.17±0.06	[4]	1	0.69	146.9	4.06±0.20
847.29±0.01	4	0	0.00	146.9	60.67±0.30	994.66±0.01	4	0	0.00	146.9	52.25±0.30
851.10±0.06	[6]	1	0.75	146.9	2.01±0.11	1007.97±0.07	[4]	1	0.73	146.9	3.86±0.20

B. Average parameters and parity assignment

No direct evidence is available to decide on the parity of the resonances, since the shape asymmetry of the resonances could not be used because of the weak potential scattering interference term. Therefore we have attempted to distinguish between $l=0$ and $l=1$ resonances on the basis of their neutron widths. This approach, already described by Bollinger and Thomas [50], and recently applied, for example, in Ref. [51], is based on the large difference in the penetrability factor for *s* and *p* waves. Assuming that neutron waves with an orbital momentum $l>1$ are not detected in the current energy range, the probability that a resonance is a *p* wave, given its value of $g\Gamma_n$, i.e., $P(l=1|g\Gamma_n)$, can be expressed with Bayes' theorem of conditional probabilities as

$$P(l=1|g\Gamma_n) = \frac{P(l=1)P(g\Gamma_n|l=1)}{P(l=0)P(g\Gamma_n|l=0)+P(l=1)P(g\Gamma_n|l=1)} = \left(1+\frac{P(l=0)}{P(l=1)}\frac{P(g\Gamma_n|l=0)}{P(g\Gamma_n|l=1)}\right)^{-1}. \quad (4)$$

The quantities $P(l=0)$ and $P(l=1)$ are the *a priori* probabilities that the resonance is an *s* or a *p* wave, respectively. Assuming a level density proportional to $2J+1$, we find for the spin $I=9/2$ nucleus ^{99}Tc a ratio $P(l=0)/P(l=1)=1/2$. More in general, this ratio takes the values 1/3, 4/9, or 1/2 for target spins $I=0$, 1/2, or >1, respectively.

The probability density function of the squared decay amplitudes γ_c^2 of a single channel is within the statistical model described by the Porter-Thomas distribution [32,52], i.e., a χ^2 distribution with one degree of freedom. The reduced neutron width of an *l*-wave resonance $\Gamma_n^l \sim \gamma_n^2$ has such a single-channel distribution for target spins $I=0$ or an orbital momentum $l=0$, where the reduced neutron width is related to the observed neutron width Γ_n by

$$\Gamma_n^l = \frac{1}{v_l}\sqrt{\frac{1\ \mathrm{eV}}{E_0}}\Gamma_n, \quad (5)$$

with

$$v_0=1, \quad v_1=\frac{(kR')^2}{1+(kR')^2}, \quad (6)$$

where $k=1/\lambda\!\!\!^{-}$ is the neutron wave number. Note that the experimentally determined effective potential scattering radius R' has been used in the factors v_l, related to the penetrability.

For *p*-wave resonances of nuclei with target spin $I>0$, more channels lead to the same resonance spin *J* if $l>0$. For example in the case of ^{99}Tc with $I=9/2$, of the possible *p*-wave spins $J=3,4,5$, and 6, the spin states 4 and 5 are twofold degenerate due to two different ways of angular momentum coupling to obtain $J=4$ and 5. The reduced neutron widths of the resonances with these spins follow, in that case, a χ^2 distribution with two degrees of freedom.

In practice the spins of most resonances are unknown and the experimental observable is $g\Gamma_n$, where *g* is the statistical spin factor, defined as

$$g=\frac{2J+1}{(2s+1)(2I+1)}, \quad (7)$$

where $s=1/2$ is the spin of the neutron.

It can be shown, as described by Gyulassy *et al.* [53], under the assumption that the neutron strength function depends only on the orbital momentum and is independent of the channel spin, that the probability of having a reduced neutron width $g\Gamma_n^l$ in an interval $d(g\Gamma_n^l)$ is given by the weighted superposition of two χ^2 distributions with one and two degrees of freedom:

$$P(g\Gamma_n^l)d(g\Gamma_n^l)=\left(\alpha_{I,l}\sqrt{\frac{2}{\pi x}}+(1-\alpha_{I,l})\right)\frac{1}{2}e^{-x/2}dx, \tag{8}$$

with

$$x=\frac{g\Gamma_n^l}{\omega_{I,l}\langle g\Gamma_n^l\rangle}. \tag{9}$$

Here $\omega_{I,l}$ and $\alpha_{I,l}$ are unity for $l=0$. For $l=1$, $\omega_{I,1}$ is equal to 1, 3/4, or 2/3, and $\alpha_{I,1}$ equals 1, 2/3, or 1/2 for a target spin I equal to 0, 1/2, or $\geqslant 1$, respectively. So for *s*-wave resonances the distribution of the quantity $g\Gamma_n^l/\langle g\Gamma_n^l\rangle$ is a χ^2 distribution with one degree of freedom, while for *p* waves the effective number of degrees of freedom is between 1 and 2 for $I>0$, always under the assumption that the neutron widths do not depend on the channel spin. The average reduced neutron width $\langle g\Gamma_n^l\rangle$ is related to the neutron strength function S_l by

$$S_l=\frac{\langle g\Gamma_n^l\rangle}{(2l+1)D_l}, \tag{10}$$

with D_l the average level spacing for resonances with orbital momentum l.

From the above it follows that the ratio of the probabilities of the neutron widths for a given value of l can be written as

$$\frac{P(g\Gamma_n|l=0)}{P(g\Gamma_n|l=1)}=\frac{\sqrt{\dfrac{3\omega_{I,1}v_1S_1D_1}{S_0D_0}}\exp\left[-\dfrac{g\Gamma_n}{2\sqrt{E}}\left(\dfrac{1}{S_0D_0}-\dfrac{1}{3\omega_{I,1}v_1S_1D_1}\right)\right]}{\alpha_{I,1}+(1-\alpha_{I,1})\sqrt{\dfrac{\pi g\Gamma_n}{6\omega_{I,1}v_1S_1D_1\sqrt{E}}}}, \tag{11}$$

i.e., expressed in terms of level spacings and neutron strength functions. The estimation of the neutron strength functions and level densities from a set of resonances can be done in several ways [54]. The most straightforward method consists of determining the slope of the cumulative number of levels as a function of the neutron energy, which gives the level density or its reciprocal, the level spacing. In the same way the cumulative sum of reduced neutron widths is related to the neutron strength function, as can be seen from Eq. (10). The drawback of this method is that many weak levels are not included to which especially the estimation of the level spacing is sensitive. Therefore, more reliable methods take into account the missing levels [55].

We have used the computer code ESTIMA [56] to estimate the average parameters D_0, S_0, and S_1. The level spacing for *p*-wave resonances D_1 was taken as $D_0/2$, assuming a level density with a $2J+1$ spin dependence [48]. The estimation procedure in this code uses methods based on the truncated Porter-Thomas distribution to account for missing levels. The number of resonances $N(x_t)$ with the same orbital momentum, having a value x from Eq. (9) larger than a threshold x_t, is given by integrating Eq. (8),

$$\begin{aligned}N(x_t)&=N_0\int_{x_t}^{\infty}P(x)dx\\&=N_0\{(1-\alpha_{I,l})e^{-x_t/2}+\alpha_{I,l}[1-\mathrm{erf}(\sqrt{x_t/2})]\},\end{aligned} \tag{12}$$

where N_0 is the unknown true number of resonances in the energy interval. The level density and neutron strength function can be fitted from the experimental data for different thresholds. By iterating the code until convergence, we obtained a value of $D_0=12.0\pm1.3$ eV for the *s*-wave level spacing, and the neutron strength function was found to be $S_0=(0.52\pm0.08)\times10^{-4}$. These values are in agreement with previous estimations for ^{99}Tc [1].

For *p* waves the situation is less straightforward. As with *s* waves, resonances with low values of the reduced neutron width are missed, but in addition the higher reduced neutron widths suffer from the diffuse limit between small *s*-wave and large *p*-wave resonances. For the neutron strength function of *p*-wave resonances we determined, in accordance with the present capabilities of the code ESTIMA, two values of S_1, using a χ^2 distribution with one and two degrees of freedom. We took the weighted average and included the difference in the assigned uncertainty to obtain the value $S_1=(3.8\pm0.8)\times10^{-4}$. This error includes only contributions due to the procedure used.

These numbers were then used to make a final division between *s*- and *p*-wave resonances using Eq. (4). If $P(g\Gamma_n|l=0)=P(g\Gamma_n|l=1)$, the probability $P(l=1|g\Gamma_n)$ equals 2/3. Therefore we assigned $l=0$ for resonances having $P(l=1|g\Gamma_n)<2/3$ and $l=1$ for the others. In Table II the assignments of the parity following this procedure are given together with the probability $P(l=1|g\Gamma_n)$. It should be noted that this division is made only in order to have a statistically coherent set of resonances for practical use. The assigned orbital momentum for individual resonances should be interpreted with care.

In Fig. 4 we show the value of $g\Gamma_n$ for the resonances together with the average value based on the estimated

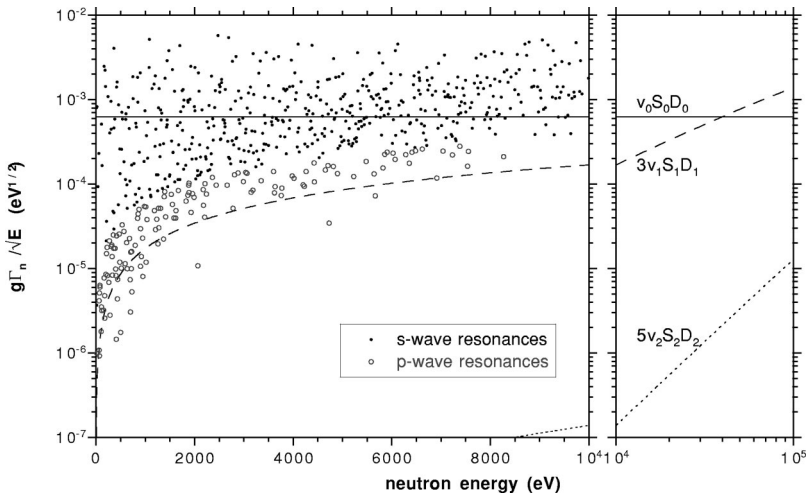

FIG. 4. The neutron widths $g\Gamma_n$ of the resolved resonances up to 10 keV, divided in *s*- and *p*-wave resonances together with the expected average value $\langle g\Gamma_n/\sqrt{E}\rangle=(2l+1)v_lS_lD_l$ for *s*-, *p*-, and *d*-wave resonances using $S_0=0.52\times10^{-4}$, $S_1=3.8\times10^{-4}$, $S_2=1\times10^{-4}$, and $D_0=12.0$ eV. The factors v_l are defined in Eq. (6).

strength functions. For comparison, the average $g\Gamma_n$ for *d* waves is also given, using a value $S_2=1\times10^{-4}$ in this mass region [1]. From Fig. 4 it can be seen that it is justified to consider that resonances with $l\geqslant2$ are not observed in the studied resolved energy range.

In reality the condition $P(g\Gamma_n|l=0)=P(g\Gamma_n|l=1)$, separating *s*- and *p*-wave resonances, corresponds to a diffuse region rather than to a line. Moreover, the uncertainties in the strength functions, level densities, and neutron widths used are not propagated, which may also influence the parity assignment.

In Fig. 5 the number of assigned *s*-wave resonances between 0 and 5 keV are shown in a cumulative plot in the sense as defined in Eq. (12). For comparison the theoretical curve is shown in the same graph. The difference at small reduced neutron widths due to missing levels is clearly visible.

A histogram of the observed distribution of the level spacing of the *s*-wave resonances between 0 and 5 keV is shown in Fig. 6. This distribution is in good approximation described by a Wigner distribution. Since the *s* waves have two possible spins, the Wigner distribution for a two-spin sequence is also shown. Due to missing levels the correspondence for small spacings is not as good as for higher spacings, where the agreement is much better.

C. Discussion of uncertainties on the resonance parameters

The uncertainties for Γ_n and Γ_γ given in Table II are the statistical uncertainties, as they result from the covariance

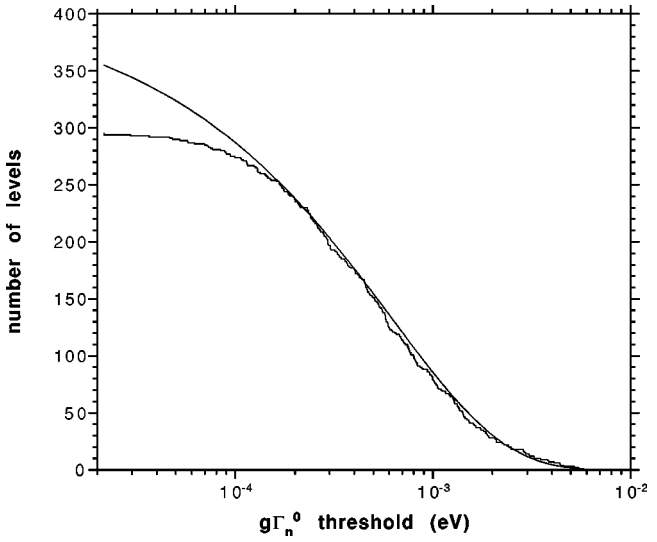

FIG. 5. The number of *s*-wave levels between 0 and 5 keV with a reduced neutron width larger than a threshold value as a function of the threshold. The smooth curve is not a fit, but shows the calculated value using the adopted valued $S_0=0.52\times10^{-4}$ and $D_0=12.0$ eV.

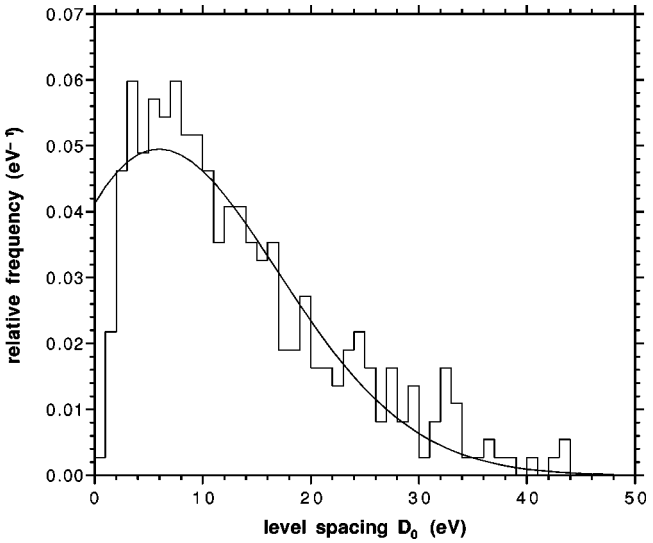

FIG. 6. The distribution of the next-neighbor level spacing of *s*-wave levels between 0 and 5 keV. The smooth curve corresponds to the Wigner distribution for a mixed sequence for two spin values [32].

matrix of the nonlinear least squares fit from REFIT. Several elements contribute to systematic uncertainties. The resolution function employed in the fits [27,28,38] is used as it is, and uncertainties resulting from an incomplete description of it are not taken into account.

The total mass of Tc in the samples has been determined very precisely, and we have neglected its uncertainty and in accordance the uncertainty on the average thickness of the samples. However, the distribution of the thickness over the sample surface is not homogeneous. The samples, prepared by pressing powdered material into pallets, have a thickness at the center which is slightly larger than on the edges. Assuming that this variation in thickness corresponds to the same variation in areal density, as a function of the transmission we calculated the ratio between the transmission of an exactly homogeneous sample and a sample of the same mass with a radial gradient in areal density corresponding to this variation. This ratio deviated from unity as a function of the transmission coefficient, and was of the order of 10^{-4} for a transmission of $T=0.01$, and much lower for higher values of T. This effect, and effects related to an inhomogeneous distribution of the sample volume, was considered negligible on the error contribution of the neutron widths.

We confirmed the length of our flight path with a transmission experiment with ^{238}U, using several sharp resonances as energy standards. We assigned an uncertainty of 1 cm to the flight path length, which also covers the reported uncertainties on the resonance energies of ^{238}U. This uncertainty is included in the errors quoted in the tables.

From Eq. (1) it can be seen that other sources of systematic errors are due to normalization and background subtraction. In order to obtain an estimate for the uncertainty on the normalization, for each in-out cycle we calculated the ratio of the monitor counts. This ratio is expected to be constant since each cycle is defined by a fixed number of counts in the detector. Normalizations based on the different monitors were all consistent within the attributed uncertainty. We checked the sensitivity of the fits of the neutron widths to the normalization by varying the normalization by one standard deviation, and then fitting the neutron widths.

In the same way we studied the influence of a variation in the background on the neutron widths. Especially resonances

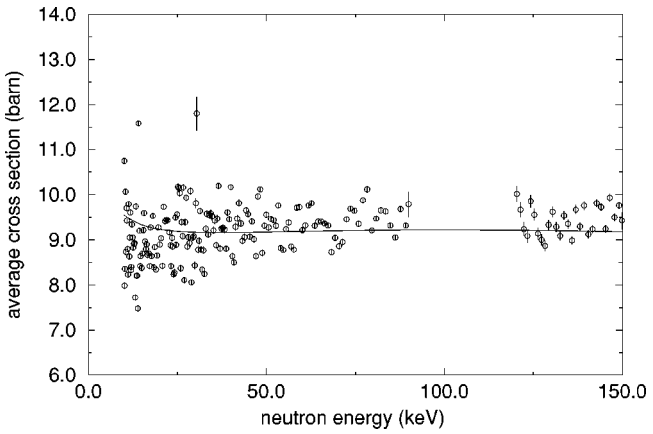

FIG. 7. The averaged measured total cross section points, shown with their statistical error bars, and the result of a fit with the code FITACS, from data of the sample with a thickness of 4.0 g/cm^2 in an energy range from 10 to 150 keV.

TABLE III. Comparison of the resonance parameters and the calculated radiative kernel of the first two *s*-wave resonances for the main neutron data libraries, four previous measurements, and the present work. See the text and references for the meaning of the quoted uncertainties.

Reference	E_0 (eV)	J	Γ_γ (meV)	$g\Gamma_n$ (meV)	$A_\gamma=\frac{g\Gamma_n\Gamma_\gamma}{\Gamma}$ (meV)
[64]	5.62	5	177.0	1.75	1.72
[42]	5.60	4	134.0	2.25	2.17
[40]	5.62	5	177.0	1.75	1.72
[41]	5.59	5	168.1	1.88	1.85
[16]	5.6	5	134.0±4.0	2.39±0.20	2.32
[17]	5.6	5	134.0±4.0	2.39±0.20	2.32
[18]	5.65	5	263.0±6.4	1.53±0.42	1.51
[20]	5.59	5	168.1±4.5	1.89±0.09	1.85
Present work	5.58	5	146.4±0.9±10.3	1.89±0.01±0.07	1.85
[64]	20.33	5	147.0	3.60	3.45
[42]	21.10	4	150.0	3.70	3.51
[40]	20.33	4	147.0	3.60	3.42
[41]	20.32	4	169.3	3.43	3.28
[16]	20.3	4	140.0±7.0	3.37±0.06	3.19
[17]	21.10	4	150.0±30.0	3.33±0.54	3.17
[18]	20.3	4	263.9±9.8	2.92±0.76	2.85
[20]	20.32	4	169.3±3.9	3.02±0.03	2.91
Present work	20.27	4	154.8±0.8±10.8	3.75±0.01±0.13	3.56

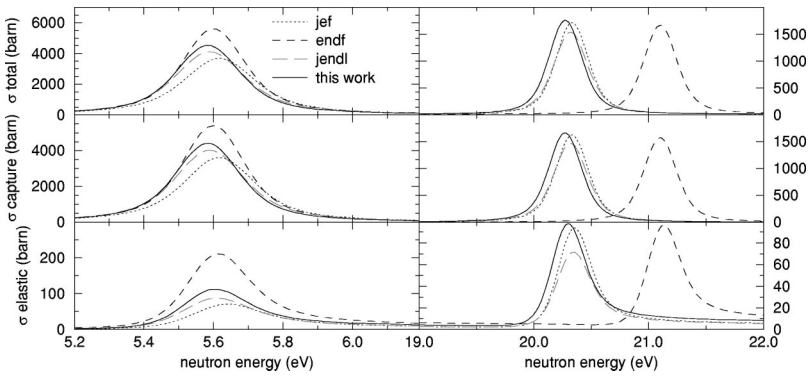

FIG. 8. The neutron capture, scattering, and total cross sections of ^{99}Tc at 300 K for the two first large resonances calculated from the resonance parameters of this work and of the three main neutron libraries.

with large transmissions were very sensitive to the applied background, due to the small signal-to-noise ratio in the dips of the resonances.

A supplementary source of uncertainty is due the radiation width, which was kept constant in the analysis for most of the resonances. We applied a 7% variation, which is the standard deviation of the fitted values of Γ_γ, on the radiation width, and observed the fitted value of the neutron widths. We estimated a systematic error of 3% from the combination of the above mentioned effects.

By comparing the results of the analysis of the data for the samples with different thicknesses, for each resonance we calculated the root-mean-squared neutron width, weighted by the statistical error. This quantity was at maximum 2%. Since it is not obvious *a priori* to what degree this scatter is correlated to the sources of uncertainty described above, or to other sources of systematic uncertainty like a difference in the energy profile of the incident neutron beam in the summed in and out spectra, we consider this as an independent supplementary error. In view of these considerations we adopted a global systematic uncertainty of 3.5% on the neutron width.

IV. ANALYSIS OF THE UNRESOLVED RESONANCES

Although resonance structures are still visible above 10 keV, resonances are very much overlapping, and in the present analysis an energy region from 10 keV up to about 150 keV was considered to be the unresolved resonance range in our measurement. The possible reactions here for ^{99}Tc are radiative capture and elastic scattering. The first inelastic scattering channel opens for the $7/2^+$ level at 140 keV. Before analyzing the data in terms of average parameters, we calculated the total cross section from the transmission data. Since in the unresolved resonance range the spacing is very small, and therefore the overlap of the resonances is large, the measured quantity is a resonance-averaged transmission. The relation between the averaged transmission and the averaged total cross section can be written as

$$\langle T\rangle=\langle e^{-n\sigma}\rangle=e^{-n\langle\sigma\rangle}\langle e^{-n(\sigma-\langle\sigma\rangle)}\rangle, \tag{13}$$

where the brackets indicate the average value. The second term on the right-hand side of this equation is a correction term due to the fluctuations of the cross section. This factor has to be calculated using level statistics. We have used the Monte Carlo code SESH [57], which takes into account the sample geometry and uses average resonance parameters to determine the correction. In this way, the calculated correction factor turned out to be quite small for the used transmission sample; it was 1.006 at 10 keV, and decreased to 1.001 at 150 keV.

The obtained averaged cross section can be described in terms of level-statistical parameters using Hauser-Feshbach calculations [58]. A detailed description of the principles and the application to ^{238}U can be found in Ref. [59].

We have used the code FITACS [60], which is well suited for this purpose for the analysis of the ^{99}Tc data from 10 keV up to 150 keV. The parameters that can be adjusted in this code are the neutron strength function S_l, the level spacing D_l, the average radiation width $\langle\Gamma_{\gamma,l}\rangle$, and a parameter R_l^∞ related to the effective potential scattering radius R_l' for each partial wave l. In this energy region it is sufficient to use the first three partial waves where the d-wave parameters are the least sensitive. For the input parameters we took the neutron strength function S_0 for s waves derived from the resolved resonance region. The neutron strength function for d waves was fixed at $S_2=1\times10^{-4}$. For the level spacing we took fixed values of $D_1=D_0/2$ and $D_2=D_0/3$ where D_0 was taken from the resolved low-energy range. Further we assumed a constant average radiation width of 150 meV at zero energy for the s, p, and d waves. The effective potential scattering radius for s waves was fixed at $R_0'=R'$, since partial waves $l\geqslant1$ do not contribute substantially to the value found at low energies.

Given these input parameters, we fitted the neutron strength function S_1 for p waves and the potential scattering radius R_1' for p waves, keeping the other parameters fixed. The results from the fit with their statistical errors were $S_1=(4.3\pm0.1)\times10^{-4}$ and $R_1'=5.6\pm0.5$ fm, with a correlation coefficient of -0.5. The sensitivity of these values to the input parameters was found to the most important for variations of S_0. Taking into account the uncertainty of S_0, a supplementary error of 9% has to be added to both the uncertainties of S_1 and R_1'.

The estimated value of $10^4S_1=4.3\pm0.4$ in this unresolved region is in agreement with the value of $10^4S_1=3.8$

± 0.8 extracted from the resolved resonance region, given in the preceding paragraph. Although *p*-wave strength functions calculated within the optical model as presented in Ref. [1] show higher values in the mass $A=100$ region, a large scatter of the value $10^4 S_1$ exists for neighboring nuclei, going from 3.6 ± 0.6 for ^{98}Mo to 8.7 ± 2.8 for ^{96}Mo. A third way to derive a value for S_1 are microscopic optical-model calculations [61,62]. Such calculations performed for ^{100}Ru, the even-even core of ^{99}Tc, give a total cross section of 10.1 b at 10 keV, in good agreement with the total cross section of ^{99}Tc shown in Fig. 7, $S_0=1.2\times 10^4$ and $S_1=3.5\times 10^4$ [63]. It should be mentioned that the penetrabilities in these calculations as well as in other evaluations are based on a nuclear radius $R=1.35A^{1/3}=6.3$ fm, while in the code FITACS they are based on a channel radius $R_c=1.23A^{1/3}+0.8=6.5$ fm, which results in an 8% lower value of S_1 from FITACS. In the resolved resonance region at low energies, the penetrabilities were calculated with an effective potential scattering radius $R'=7.17$ fm. This choice also affects the determination of S_1. The extension of the energy range of the total cross section measurements to much higher energies would give more precise information on the neutron strength functions and could in addition refine optical-model calculations.

In Fig. 7 the fitted average cross section is shown, together with the averaged pointwise data. Due to the sulphur filter which was kept permanently in the neutron beam for its large resonances in the vicinity of 150 keV, the data in this region cannot be used and have been left out of the analysis.

V. COMPARISON AND CONCLUDING REMARKS

For comparison of the present work with existing data, in Table III we give the resonance parameters of the first two large *s*-wave resonances at 5.6 and 20.3 eV and the radiative kernel $A_\gamma=g\Gamma_n\Gamma_\gamma/(\Gamma_n+\Gamma_\gamma)$ calculated from them, together with the values of previous measurements and the currently used libraries with evaluated nuclear data. The Russian evaluated neutron data library BROND-2.2 [64] contains 107 resonances up to 1.4 keV, ENDF/B-VI [42] has 68 resonances up to 800 eV, and JEF-2.2 [40] has 89 resolved resonances below 1.2 keV. Finally JENDL-3.2 [41] seems the most complete, with 341 resonances resolved up to 4.2 keV. The Chinese evaluated neutron data library CENDL-2.1 [65] does not contain data for ^{99}Tc. The present work contains 659 resonances up to 10 keV. In Fig. 8 the calculated neutron total, capture and elastic cross section are shown for the results of the present work, together with the data from the main neutron libraries.

Besides the results presented herein for the transmission experiments in the resolved resonance region, capture experiments have also been performed in the same energy range from 3 eV up to 150 keV [66]. These data are currently under analysis. A simultaneous analysis of the data of this transmission experiment and the capture experiment is expected to improve the quality of the resonance parameters.

ACKNOWLEDGMENTS

The authors want to thank ITU Karlsruhe for providing the technetium, C. Ingelbrecht for preparing the samples, the IRMM Linac operators for providing the neutron beam for these measurements, and H. Weigmann, D. Paya, and H. Tellier for valuable discussions. We also express our gratitude to E. Fort and O. Bouland for their help with the code ESTIMA, and M. C. Moxon for advice on using his code REFIT.

[1] S. F. Mughabghab, M. Divadeenam, and N. E. Holden, *Neutron Cross Sections; Neutron Resonance Parameters and Thermal Cross Sections* (Academic, New York, 1981).
[2] S. Sukhoruchin, Z. N. Soroko, and V. V. Deriglazov, in *Low Energy Neutron Physics: Tables of Neutron Resonance Parameters*, edited by H. Schopper, Landolt-Bornstein, New Series, Group I, Vol. 16 (Springer, New York, 1998).
[3] C. D. Bowman, Annu. Rev. Nucl. Part. Sci. **48**, 505 (1998).
[4] M. Salvatores, I. Slessarev, and A. Tchistiakov, Nucl. Sci. Eng. **130**, 309 (1998).
[5] R. J. M. Konings, J. L. Kloosterman, J. A. Hendriks, and H. Gruppelaar, Nucl. Sci. Eng. **128**, 70 (1998).
[6] H. Gruppelaar, J. L. Kloosterman, and R. J. M. Konings, Advanced Technologies for the Reduction of Nuclear Waste, Report No. ECN-R-98-008, 1998.
[7] Z. N. Soroko and S. Sukhoruchin, in *Proceedings of the VI International Seminar on the Interaction of Neutrons with Nuclei*, edited by W. I. Furman *et al.* (JINR, Dubna, 1998), p. 141.
[8] J. D. Bowman, G. T. Garvey, and M. B. Johnson, Annu. Rev. Nucl. Part. Sci. **43**, 829 (1993).
[9] H. Postma, F. Gunsing, and F. Corvi, Phys. Rev. C **53**, R558 (1996).
[10] F. Käppeler, H. Beer, and K. Wisshak, Rep. Prog. Phys. **52**, 945 (1989).
[11] G. Wallerstein, I. Iben, Jr., P. Parker, A. Merchant-Boesgaard, G. M. Hale, A. E. Champagne, C. A. Barnes, F. Käppeler, V. V. Smith, R. D. Hoffman, F. X. Timmes, C. Sneden, R. N. Boyd, B. S. Meyer, and D. L. Lambert, Rev. Mod. Phys. **69**, 995 (1997).
[12] M. Busso, R. Gallino, D. L. Lambert, C. M. Raiteri, and V. V. Smith, Astron. J. **399**, 218 (1992).
[13] R. R. Winters and R. L. Macklin, Astron. J. **313**, 808 (1987).
[14] N. J. Pattenden, Proc. Geneva Conf. **16**, 44 (1958).
[15] G. G. Slaughter, J. A. Harvey, R. C. Block, and G. L. Jenkins, Bull. Am. Phys. Soc. **3**, 364 (1958).
[16] T. Watanabe and S. D. Reeder, Nucl. Sci. Eng. **41**, 188 (1970).
[17] Yu. V. Adamchuck, G. V. Muradyan, Yu. G. Shchenkin, and M. A. Voskanyan, Report No. IAE-2335, 1973.
[18] Jen-Chang Chou and H. Werle, J. Nucl. Energy **27**, 811 (1973).
[19] R. C. Little and R. C. Block, Trans. Am. Nucl. Soc. **26**, 574 (1977).

[20] P. Fischer, U. Harz, and H. G. Priesmeyer, Atomkern. Kerntech. **38**, 63 (1981).
[21] R. L. Macklin, Nucl. Sci. Eng. **81**, 520 (1982).
[22] H. A. J. van der Kamp and H. Gruppelaar, Report No. ECN-RX-92-023, 1992.
[23] J. Rowlands, OECD/NEA High Priority Nuclear Data Request List (Nuclear Energy Agency, Issy-les-Moulineaux, 1998).
[24] J. M. Salomé and R. Cools, Nucl. Instrum. Methods **179**, 13 (1981).
[25] J. M. Salomé, Physicalia **8**, 261 (1986).
[26] D. Tronc, J. M. Salomé, and K. H. Böckhoff, Nucl. Instrum. Methods Phys. Res. A **228**, 217 (1985).
[27] A. Brusegan, G. Rohr, R. Shelley, E. Macavero, C. van der Vorst, F. Poortmans, L. Mewissen, and G. Vanpraet, in *Proceedings of the International Conference on Nuclear Data for Science and Technology*, Gatlinburg, Tennessee, 1994, edited by J. K. Dickens (American Nuclear Society, La Grange Park, IL, 1994), p. 224.
[28] A. Brusegan, E. Macavero, and C. van der Vorst, in *Proceedings of the International Conference on Nuclear Data for Science and Technology* [27], p. 227.
[29] C. Bastian, IEEE Trans. Nucl. Sci. **43**, 2343 (1996).
[30] C. Bastian, in *Proceedings of the International Conference on Neutron Research and Industry, Crete, Greece*, 1996, edited by George Vourvopoulos (Society of Photo-optical Instrumentation Engineers, Bellingham, WA, 1997), p. 611.
[31] A. M. Lane and R. G. Thomas, Rev. Mod. Phys. **30**, 257 (1958).
[32] J. E. Lynn, *The Theory of Neutron Resonance Reactions* (Oxford University, Oxford, 1968).
[33] F. H. Fröhner, Report No. KfK-5073, 1992.
[34] A. A. Luk'yanov and N. B. Yaneva, Phys. Part. Nuclei **28**, 331 (1997).
[35] *Experimental Neutron Resonance Spectroscopy*, edited by J. A. Harvey (Academic, New York, 1970).
[36] A. Foderaro, *The Elements of Neutron Interaction Theory* (Maple Press, Cambridge, MA, 1971).
[37] M. C. Moxon and J. B. Brisland, *REFIT, A Least Squares Fitting Program for Resonance Analysis of Neutron Transmission and Capture Data Computer Code* (United Kingdom Atomic Energy Authority, Harwell, 1991).
[38] M. C. Moxon (private communication).
[39] W. E. Lamb, Phys. Rev. **55**, 190 (1939).
[40] C. Nordborg and M. Salvatores, *Status of the JEF Evaluated Data Library*, Nuclear Data for Science and Technology, edited by J. K. Dickens (American Nuclear Society, LaGrange, IL, 1994).
[41] T. Nakagawa *et al.*, J. Nucl. Sci. Technol. **32**, 1259 (1995).
[42] Cross Section Evaluation Working Group, *ENDF/B-VI Summary Documentation*, Report BNL-NCS-17541 (ENDF-201), edited by P. F. Rose, National Nuclear Data Center, Brookhaven National Laboratory, Upton, NY (1991).
[43] F. W. Mosteller and J. W. Tukey, *Data Analysis and Regression* (Addison-Wesley, Reading, MA, 1977).
[44] A. Stuart and J. K. Ord, *Kendall's Advanced Theory of Statistics*, (Wiley, New York, 1994), Vol. 1.
[45] F. Gunsing, A. Leprêtre, C. Mounier, C. Raepsaet, A. Brusegan, F. Corvi, E. Macavero, L. Zanini, and H. Postma, in *6th International Seminar on Interaction of Neutrons with Nuclei*, edited by W. I. Furman *et al.* (JINR, Dubna, 1998), p. 133.
[46] L. Zanini, Ph.D. thesis, Delft University, 1998.
[47] F. Gunsing, K. Athanassopulos, F. Corvi, H. Postma, Yu. P. Popov, and E. I. Sharapov, Phys. Rev. C **56**, 1266 (1997).
[48] A. Gilbert and A. G. W. Cameron, Can. J. Phys. **43**, 1446 (1965).
[49] H. Harada, S. Nakamura, T. Katoh, and Y. Ogata, J. Nucl. Sci. Technol. **32**, 395 (1995).
[50] L. M. Bollinger and G. E. Thomas, Phys. Rev. **171**, 1293 (1968).
[51] C. M. Frankle, E. I. Sharapov, Yu. P. Popov, J. A. Harvey, N. W. Hill, and L. W. Weston, Phys. Rev. C **50**, 2774 (1994).
[52] C. E. Porter and R. G. Thomas, Phys. Rev. **104**, 483 (1956).
[53] M. Gyulassy, R. J. Howerton, and S. T. Perkins, Report No. UCRL-50400, Vol. 11, 1972.
[54] F. H. Fröhner, Report No. KfK-3553, 1983.
[55] M. S. Moore, J. D. Moses, G. A. Keyworth, J. W. T. Dabbs, and N. W. Hill, Phys. Rev. C **18**, 1328 (1978).
[56] E. Fort and J. P. Doat, ESTIMA computer code, Report No. NEANDC-161U, 1983; E. Fort, O. Bouland, and P. Long, *ibid.*, updated version, 1999.
[57] F. H. Fröhner, SESH computer code, Report No. GA-8380, 1968.
[58] W. Hauser and H. Feshbach, Phys. Rev. **87**, 366 (1952).
[59] F. H. Fröhner, Nucl. Sci. Eng. **103**, 119 (1989).
[60] F. H. Fröhner, B. Goel, and U. Fischer, FITACS computer code, Report No. ANL-83-4, 1983.
[61] E. Bauge, J. P. Delaroche, and M. Girod, Phys. Rev. C **58**, 1118 (1998).
[62] F. Maréchal, T. Suomijärvi, Y. Blumenfeld, A. Azhari, E. Bauge, D. Bazin, J. A. Brown, P. D. Cottle, J. P. Delaroche, M. Fauerbach, M. Girod, T. Glasmacher, S. E. Hirzebruch, J. K. Jewell, J. H. Kelley, K. W. Kemper, P. F. Mantica, D. J. Morrissey, L. A. Riley, J. A. Scarpaci, H. Scheit, and M. Steiner, Phys. Rev. C **60**, 034615 (1999).
[63] E. Bauge and J. P. Delaroche (private communication).
[64] A. I. Blokhin *et al.*, *Current Status of Russian Nuclear Data Libraries*, Nuclear Data For Science and Technology, edited by J. K. Dickens (American Nuclear Society, LaGrange Park, IL, 1994), Vol. 2, p. 695.
[65] Chinese Nuclear Data Center, CENDL-2, *The Chinese Evaluated Nuclear Data Library for Neutron Reaction Data*, Report No. IAEA-NDS-61, Rev. 3, 1996, International Atomic Energy Agency, Vienna, Austria.
[66] C. Raepsaet, Ph.D. thesis, University of Marseille, 1998.